TASK QUARTERLY 7 No 4 (2003), 595–610

EXPERIMENTAL AND THEORETICAL STUDIES OF RESONANCE EFFECTS DURING CONFINED FLOW IN SILOS

MACIEJ NIEDOSTATKIEWICZ AND JACEK TEJCHMAN

Faculty of Civil Engineering, Gdańsk University of Technology,
Narutowicza 11/12, 80-952 Gdańsk, Poland
mniedost@pg.gda.pl, tejchmk@pg.gda.pl

(Received 2 June 2003)

Abstract: The paper deals with experimental and theoretical research of resonance effects during silo emptying. The influence of resonance effects on wall pressures in silos has been investigated with model tests and FE analyses. The model tests were carried out with a cylindrical and rectangular silo containing various cohesive and non-cohesive bulk solids. The onset of dynamic silo flow was simulated with controlled outlet velocity along the bottom in a plane strain model and large silo. The confined flow of dry sand in a silo with parallel walls during resonance was described with a finite element method based on a polar elasto-plastic constitutive law. It differs from the conventional theory of plasticity by the presence of Cosserat rotations and couple stresses using mean grain diameter as a characteristic length. In the FE calculations, the silo walls were taken into account.

Keywords: bulk solid, cohesion, dynamic effects, finite element method, model tests, polar elasto-plasticity, resonance, silos

1. Introduction

Dynamic effects in bulk solids are an inherent characteristic of every silo discharge [1–4]. They occur in the form of pulsations and shocks. In dry granular materials (non-cohesive), only pulsations are created. In cohesive bulk solids, pulsations and shocks can be observed at the same time. Silo pulsations are connected to natural vibrations of the silo fill induced by disturbances of the flow at the silo bottom due to the outlet being smaller than the silo diameter, the hopper, or the bottom plate, slowing down the flow. The pulsations are created at the bottom and propagate upwards in the form of stress waves. At the silo bottom, a change in the direction of shear deformation is connected to local volume changes in the fill alternating from dilatancy to contractancy. The material's dilatancy results in a decrease of the vertical stress, an increase in wall pressure, and deceleration of the fill. The contractancy causes, in turn, an increase of the vertical stress, a release of the wall stresses, and acceleration of the fill. The stress changes due to the presence of inertial forces lead to dynamic pulsations. Silo shocks are created due to the formation and collapse of bridges connected to a strong change of cohesion with the material's density above

the outlet. The solid is consolidated by filling and pressurizing in the hopper and then dilated and softened near the outlet, so that the bridges break down.

Dynamic effects can be very dangerous if the frequencies of self-excited dynamic effects in bulk solids match the frequencies of natural vibrations of the silo structure and resonance effects thus occur. It is very often the case in steel and aluminium silos, whose walls are relatively thin (compared with concrete silos, see [4, 5]). The resonance phenomena take place mainly during mass flow of stiff grains in silos with smooth walls. In this case, they are directly transferred to the wall and then to the supporting structure. During channel flow in the middle of the silo, dynamic effects are damped by the material sticking to the wall. In silos with very rough walls, they are damped in the wall shear zone, where plastic deformations prevail.

The intention of the experimental and theoretical research presented in this paper was to determine the effect of resonance on wall stresses during silo emptying.

2. Model tests

Model tests were performed with a perspex cylindrical silo (height $h = 0.2$m, inner diameter $d = 0.2$m) and a perspex rectangular silo (height $h = 0.2$m, cross-section $0.15 \times 0.3\,\mathrm{m}^2$) [6, 7]. They contained various non-cohesive bulk solids: fine sand, gravel, polymer granulate, wheat, and cohesive bulk solids: sand with water, sand with glycerine and sand with clay. The emptying process was produced mainly by opening a steel plate in the silo bottom (gravitational outflow). Tests were also performed with controlled outlet velocity. During the model tests, the following quantities were measured: horizontal and vertical accelerations on the wall (also circumferential accelerations in a cylindrical silo), vertical accelerations on the upper boundary of the bulk solid, horizontal and vertical strains on the wall, and horizontal normal stresses on the wall. The model experiments were carried out with the following variable parameters:

- initial sand density, γ (loose and dense sand),
- outlet diameter, d_o, for gravitational flow ($d_o = 0.01$, 0.04, 0.07 and 0.12m),
- filling height, h ($h = 1.0$ and 2.0m),
- mean grain diameter of sand, d_{50} ($d_{50} = 0.3$, 0.8 and 3.0mm),
- grain stiffness (sand, gravel, polymer granulate and wheat),
- wall roughness (smooth, rough and very rough walls),
- velocity of the bottom plate, v, for controlled outflow ($v = 0.7$, 2.0, 4.0 and 5.0mm/s),
- cohesion (sand with water, sand with glycerine, sand with clay).

First, natural frequencies of the model silos were measured. Silos were excited by both vertical and horizontal vibration. During vertical excitation, the following natural frequencies below 100Hz were obtained in silos containing fine sand: 22, 69, 80 and 88Hz (cylindrical silo), and 19Hz (rectangular silo). The deformed cylindrical silo had the form of a barrel of varying height and diameter. In turn, bending deformations were dominant in the rectangular silo. When the silos were excited by the horizontal vibration, the following natural frequencies below 100Hz were obtained in silos containing fine sand: 11, 28, 67, 69, 72 and 87Hz (cylindrical silo), and 11, 66 and 90Hz (rectangular silo). The natural frequencies of solids in a vertical direction

were in the range of basic frequencies calculated from the equation for the fundamental frequency of longitudinal wave propagation in an elastic bar:

$$f = \sqrt{\frac{E(1-v)}{\rho(1+v)(1-2v)}}/2h = \frac{v_c}{2h} = \frac{200}{4.0} = 50\,\text{Hz (at end conditions free-free)}, \quad (1)$$

$$f = \sqrt{\frac{E(1-v)}{\rho(1+v)(1-2v)}}/4h = \frac{v_c}{4h} = \frac{200}{8.0} = 25\,\text{Hz (at end conditions fixed-free)}, \quad (2)$$

where v_c – velocity of the longitudinal compressive stress wave, $E = 50\,\text{MPa}$ (elastic modulus of sand), $v = 0.3$ (Poisson's ratio of sand), $h = 2.0$ (silo height) and $\rho \approx 1700\,\text{kg/m}^3$ (mass density of sand).

The tests with sand in the cylindrical silo (with gravitational flow) showed that strong acoustic dynamic pulsations occurred from the beginning of the emptying process independently of the outlet's diameter and sand density. In the cylindrical silo, pulsations were registered only in the upper region of the cylinder (0.8–1.0 m above the bottom) during plug flow. Later, channel flow in the middle of the solid occurred. The tests with sand in a rectangular silo during gravitational flow showed that the resonance effects appeared only in tests with dense sand during channel flow occuring directly at the wall.

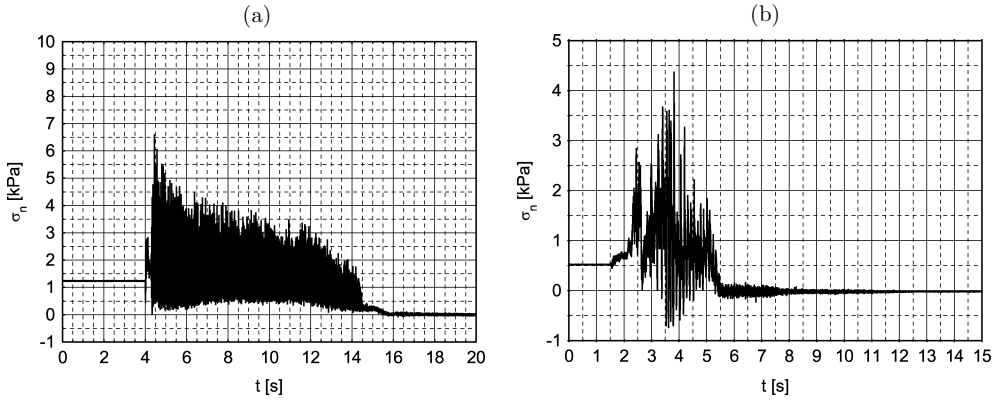

Figure 1. Measured horizontal wall pressure, σ_n, at $h = 1.0\,\text{m}$ during time of flow, t: (a) cylindrical silo – loose sand, $d_0 = 0.07\,\text{m}$; (b) rectangular silo – dense sand, $d_0 = 0.12\,\text{m}$ ($d_{50} = 0.8\,\text{mm}$, smooth walls)

The maximum wall pressures during resonance were about $\sigma_n = 6.5$–$7\,\text{kPa}$ (Figure 1). They were 2–3 times higher than those calculated with silo standards (with the aid of a Janssen equation). The lowest frequency of wall vibrations was equal to the basic frequency of natural vibrations of the silo structure in the vertical direction. For more detailed discussion of the tests the reader is referred to [6, 7].

A controlled outlet velocity (in the considered range of v) influenced slightly the amplitudes of vertical accelerations but it did not influence wall pressures (Figure 2). During tests with $v = 0.7$–$5.0\,\text{mm/s}$, the maximum vertical accelerations on the wall, a_v, were $\pm(0.5$–$3.0)\,\text{m/s}^2$. The maximum wall pressures increased during flow to 1.0 kPa. The frequencies of wall vibrations were similar to those observed during gravitational flow.

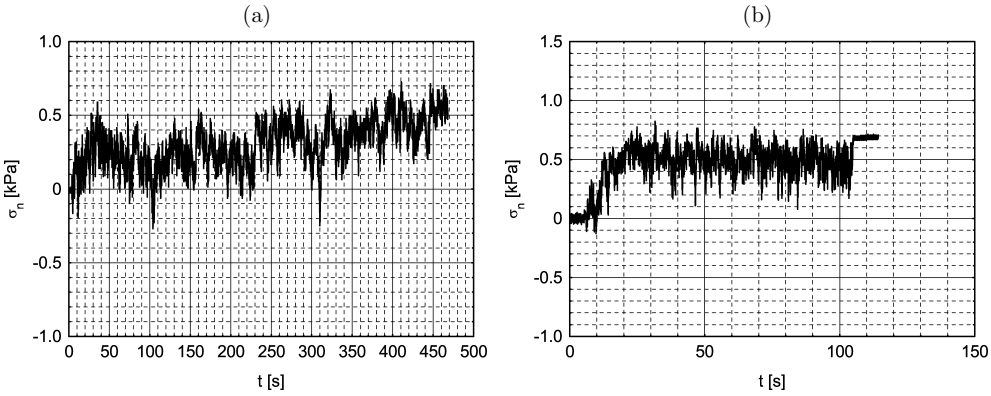

Figure 2. Measured horizontal wall pressure, σ_n, at $h = 1.0$m for controlled outlet velocity: (a) $v = 0.7$mm/s; (b) $v = 5$mm/s (cylindrical silo, loose sand, $d_{50} = 0.8$mm, smooth walls)

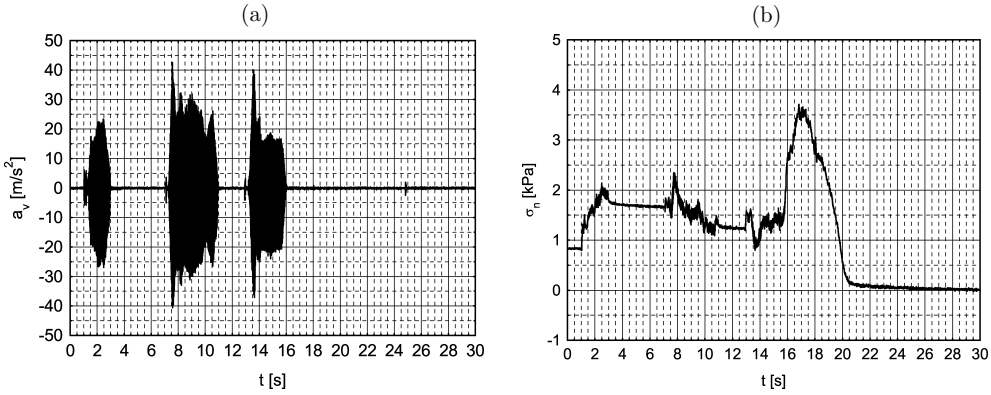

Figure 3. Measured: (a) vertical acceleration a_v on the wall and (b) horizontal wall pressure σ_n at $h = 1.0$m (cylindrical silo, mixture of sand and water, $d_0 = 0.12$m, smooth walls)

During silo tests with cohesive mixtures, both pulsations and non-regular shocks were observed. The flow took place by jumps due to the formation and collapse of arches. The effect of cohesion on accelerations and pressures was great. For a mixture of sand and water, the strongest dynamic effects occurred at $d_o = 0.12$m and cohesion $c = 0.18$kPa. In this case, the maximum vertical accelerations on the wall, a_v, were 40m/s^2 (Figure 3a) and the maximum wall pressures were 3.5kPa (Figure 3b). The frequency of pulsations and shocks was equal to 60Hz and 0.8Hz, respectively. For $d_o = 0.07$m, wall pressures were smaller by about 20%.

For a mixture of sand with glycerine (0.05% of volume), the maximum vertical accelerations on the wall were about 30m/s^2 (Figure 4a). The maximum wall pressures were 1.6kPa (Figure 4b). When the volume contents of glycerine was 0.08–0.09%, the maximum vertical accelerations on the wall were $50\text{–}60\text{m/s}^2$ (Figures 4c and 4e), and the maximum wall pressures were 2.3kPa (Figures 4d and 4f). The frequency of pulsations was equal to 60Hz, the frequency of shocks was 1Hz.

In the case of a mixture of sand and clay ($< 4\%$ of volume), only short dynamic pulsations appeared. The maximum vertical accelerations on the wall were 10m/s^2 (Figure 5a). The wall pressures increased during flow by 20% only (in spite of the

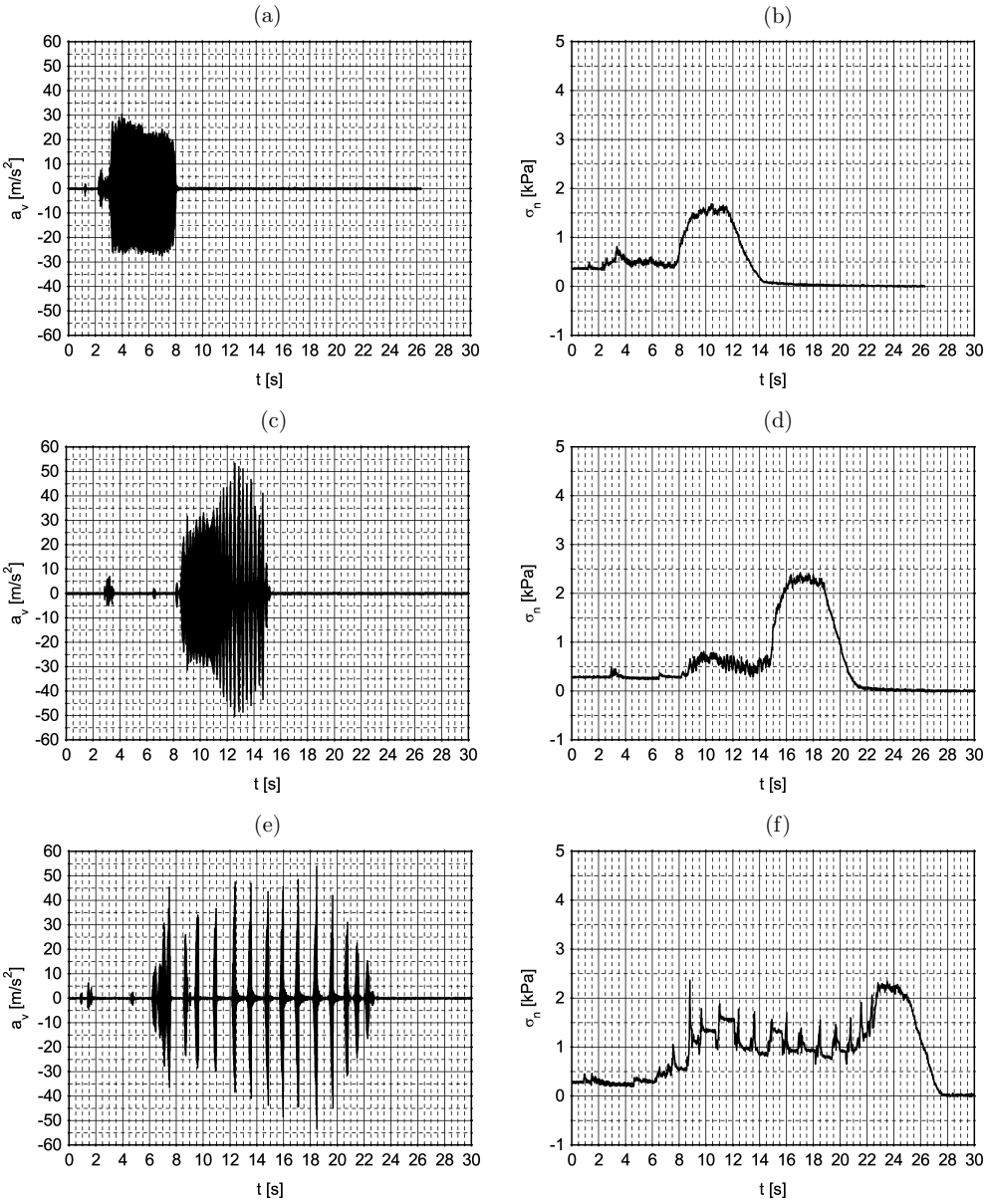

Figure 4. Measured vertical acceleration, a_v, on the wall and horizontal wall pressure, σ_n, at $h = 1.0$m: (a) and (b) 0.05% volume, (c) and (d) 0.08% volume, (e) and (f) 0.09% volume (cylindrical silo, mixture of sand and glycerine, $d_0 = 0.07$m, smooth walls)

short resonance) compared to static pressure (Figure 5b). When the contents of clay was over 4%, flow did not occur due to arching.

The experimental results from model silos cannot be directly applied to large silos due to scale effects caused by the pressure level (influencing both the internal wall friction and the dilatancy angle of bulk solids), the ratio between the mean grain diameter and the silo diameter, and the volume of the bulk solid damping dynamic effects [4, 8].

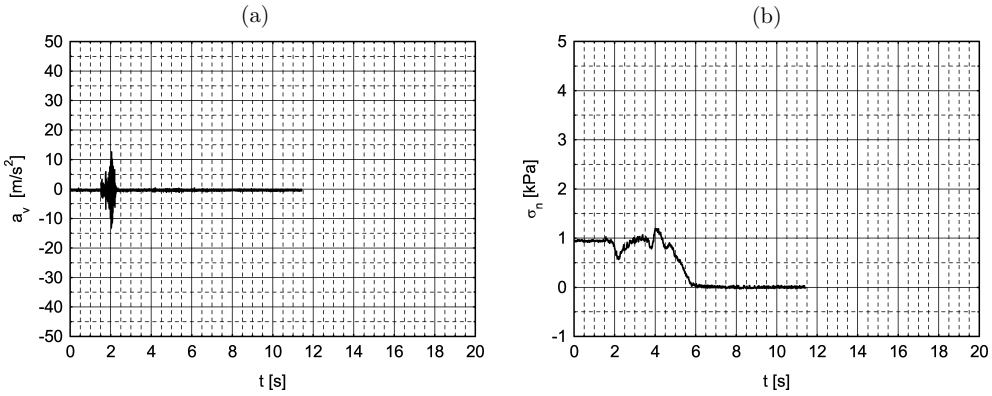

Figure 5. Measured: (a) vertical acceleration, a_v, on the wall and (b) horizontal wall pressure, σ_n, at $h = 1.0$m (cylindrical silo, mixture of sand and clay, $d_0 = 0.12$m, smooth walls)

3. Method of resonance reduction

The favoured method of suppressing dynamic effects in silos has been to increase of the roughness of walls [7]. This method is effective both for cohesive and non-cohesive bulk solids. The maximum registered wall accelerations in a cylindrical silo with very rough walls and dry loose sand in all directions were smaller than $1\,\mathrm{m/s^2}$ [5, 6]. The wall pressures in a cylindrical silo during emptying were smaller than 1.8kPa. The basic frequency of pulsations was about 200Hz. A noticeable shear zone with a thickness of about 20mm developed along very rough walls. Mass flow still took place in the upper part of the silo but the material moved slightly faster beyond the shear zone than along the walls. The formation of shear zone contributed to a significant increase in the frequencies of pulsations, due to the presence of additional horizontal and rotational stress waves [4]. The frequency of these waves was greater than this of the longitudinal stress waves due to a shorter way of propagation. In this way, the resultant frequency of pulsations was higher and the resonance range could be avoided. Pulsations were additionally damped in the wall shear zone, where plastic shear deformations prevailed.

In the case of a mixture of sand and water ($c = 0.18$kPa), the reduction of wall pressures in a silo with very rough walls was significant (by about 60%), compared to those for smooth walls (Figure 6). When the silo contained a mixture of sand and glycerine, the reduction was similar (Figure 7b). The amplitudes of vertical accelerations on the wall were smaller than $\pm 1\,\mathrm{m/s^2}$ (Figure 7a).

In experiments with a mixture of sand and clay in a cylindrical silo with very rough walls, the maximum wall stresses increased by 30% (from 1.2kPa up to 1.6kPa, see Figure 8).

During tests in a cylindrical silo with controlled outlet velocity, very rough walls and loose sand, the maximum wall pressures were higher by 10% when compared to those of the silo with smooth walls (Figure 9).

In the case of a rectangular silo with loose sand and very rough walls, the maximum wall pressures were higher by 20% when compared to those of the silo with smooth walls (without resonance).

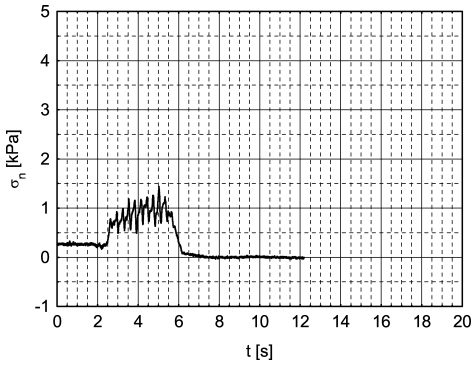

Figure 6. Measured horizontal wall pressure, σ_n, at $h = 1.0$m (cylindrical silo, mixture of sand and water, $d_0 = 0.12$m, very rough walls)

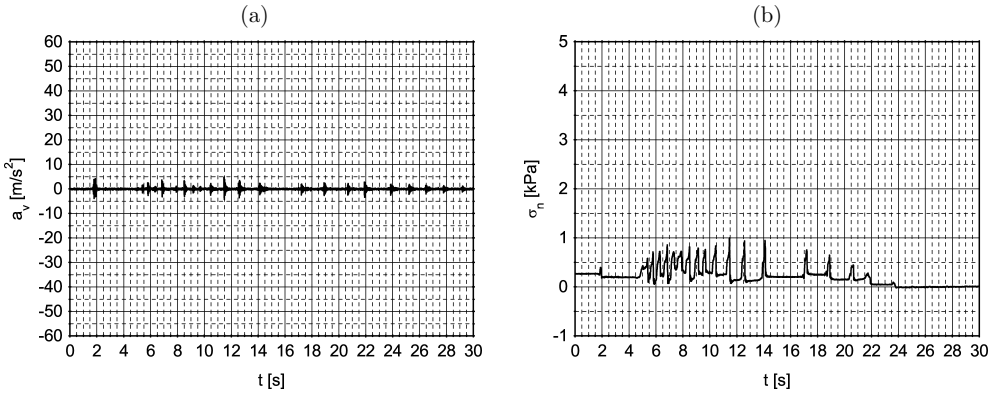

Figure 7. Measured: (a) vertical acceleration, a_v, on the wall and (b) horizontal wall pressure, σ_n, at $h = 1.0$m (cylindrical silo, mixture of sand and glycerine, $d_0 = 0.07$m, very rough walls)

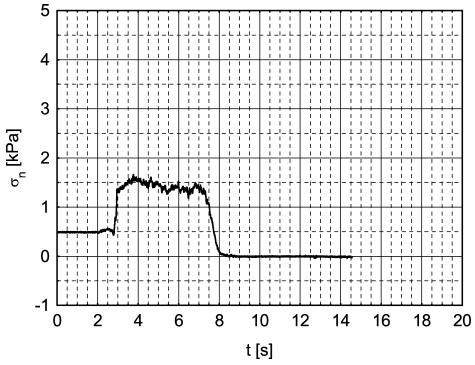

Figure 8. Measured horizontal wall pressure, σ_n, at $h = 1.0$m (cylindrical silo, mixture of sand and clay, $d_0 = 0.12$m, very rough walls)

4. Polar elasto-plastic constitutive law

The resonance effects occurring during silo emptying of granular bulk solids (non-cohesive sand) at the onset of flow were numerically analysed with an FEM and a polar elasto-plastic constitutive relation with isotropic hardening and softening

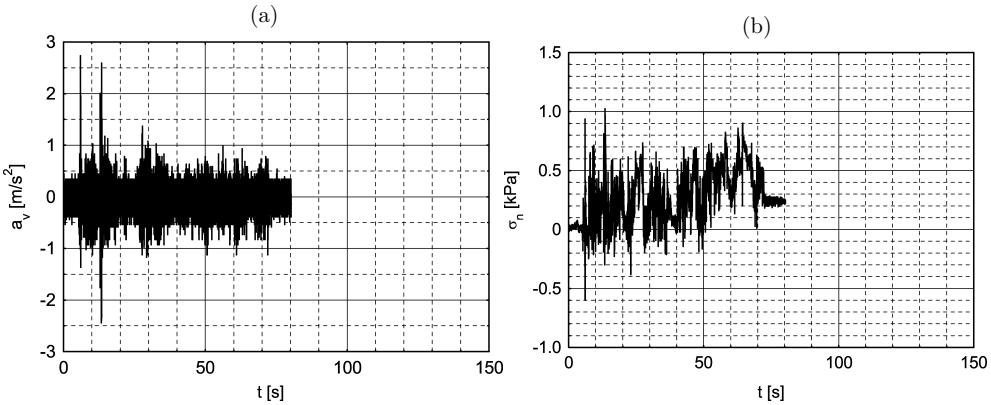

Figure 9. Measured: (a) vertical acceleration, a_v, on the wall and (b) horizontal wall pressure, σ_n, at $h = 1.0$m (cylindrical silo, loose sand, $d_{50} = 0.8$mm, controlled outlet velocity $v = 5$mm/s, very rough walls)

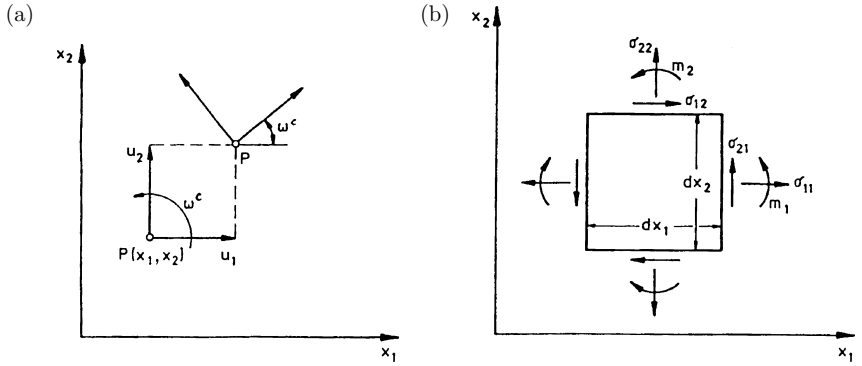

Figure 10. Plane strain Cosserat continuum: degrees of freedom (u_1, u_2 – horizontal and vertical displacement, ω^c – Cosserat rotation)

proposed by [4, 9, 10]. The constitutive law was formulated within a polar (Cosserat) continuum. A Cosserat continuum differs from a classical (non-polar) continuum in that an additional rotation, ω^c, appears in its kinematics (Figure 10a). Thus, each material point of the plane polar continuum has three degrees of freedom: two translational degrees of freedom, u_1 and u_2, and a rotational degree of freedom, ω^c. The state of deformation within a polar continuum is described by six quantities:

$$\varepsilon_{11} = u_{1,1}, \qquad \varepsilon_{22} = u_{2,2}, \tag{3}$$

$$\varepsilon_{12} = u_{1,2} + \omega^c, \qquad \varepsilon_{21} = u_{2,1} - \omega^c, \tag{4}$$

$$\kappa_1 = \omega^c_{,1}, \qquad \kappa_2 = \omega^c_{,2}, \tag{5}$$

where

$$()_{,i} = \partial()/\partial x_i. \tag{6}$$

ε_{ij} are components of the deformation tensor, and κ_i are components of the curvature vector. Normal deformations are defined similarly as in a non-polar continuum. The shear deformations ε_{12} and ε_{21} can be viewed as relative deformations relating the macro-displacement gradient and micro-rotation; in contrast to a non-polar continuum, $\varepsilon_{12} \neq \varepsilon_{21}$. The curvatures κ_1 and κ_2 describe macro-deformation gradients

of the micro-rotation. ε_{ij} and κ_i are invariant with respect to rigid body motions. Six deformation quantities are conjugate with respect to energy to six stress quantities referred to the actual configuration. The four components of ε_{ij} are associated with the four components of the stress tensor σ_{ij} which is generally non-symmetric ($\sigma_{12} \neq \sigma_{21}$). The curvatures κ_i are associated with the couple stresses m_i. Figure 10b shows the stresses, couple stresses, volume body forces, f_i^B, volume body moment, m^B, volume inertia forces, $\rho\ddot{u}_i$, and volume moment of spin inertia, $\theta\ddot{\omega}^c$, at an infinitesimal element (dx_1, dx_2) of a plane Cosserat continuum. The force equilibrium and the moment equilibrium give the following equations of motion:

$$\sigma_{11,1} + \sigma_{12,2} - f_1^B + \rho\ddot{u}_1 = 0, \tag{7}$$

$$\sigma_{21,1} + \sigma_{22,2} - f_2^B + \rho\ddot{u}_2 = 0, \tag{8}$$

$$m_{1,1} + m_{2,2} + \sigma_{21} - \sigma_{12} - m^B + \theta\ddot{\omega}^c = 0, \tag{9}$$

where

$$\ddot{()} = \partial^2 () / \partial t^2. \tag{10}$$

ρ is the mass density, and θ denotes the volume moment of inertia. The equilibrium conditions (Equations (7)–(9)) are equivalent to the virtual work principle:

$$\int_B (\sigma_{ij}\delta\varepsilon_{ij} + m_i\delta\kappa_i)dV = \int_B \left[(f_i^B - \rho\ddot{u}_i)\delta u_i + (m^B - \theta\ddot{\omega})\delta\omega^c\right] dV + \\ + \int_{\partial_1 B} t_i\delta u_i dA + \int_{\partial_2 B} m\delta\omega^c dA, \tag{11}$$

where

$$\sigma_{ij}n_j = t_i \quad \text{on} \quad \partial_1 B, \qquad m_i n_i = m \quad \text{on} \quad \partial_2 B. \tag{12}$$

t_i and m are prescribed boundary tractions and moment, respectively, $\delta\varepsilon_{ij}$ and $\delta\kappa_i$ denote virtual deformations and curvatures, δu_i is virtual displacement, $\delta\omega^c$ is the virtual Cosserat rotation, A is body surface, and V is body volume. Virtual displacements and the virtual Cosserat rotations disappear on those parts of the boundary where the kinematic boundary conditions are prescribed. The work principle states that the fields σ_{ij}, mi satisfying for arbitrary kinematically admissible virtual δu_i, $\delta\omega_c$ also satisfy the equilibrium conditions (Equations (7)–(9)) and the boundary conditions (Equation (12)). The virtual work principle is used to formulate an FEM of motion. As a consequence of the presence of rotations and couple stresses, the constitutive law for granular materials within a polar continuum is endowed with a characteristic length corresponding to the mean grain diameter. Thus, the numerical results are not sensitive to spatial discretisation and boundary value problems remain mathematically well-posed when using softening constitutive laws. A polar approach can model the thickness of shear zones and related grain size effects. In addition, the effect of the pressure level can be also considered in the constitutive law (by a decrease of both the internal friction angle and the dilatancy angle with increasing pressure and by an increase of the elastic modulus with increasing pressure).

A Cosserat elasto-plastic constitutive model for granular materials with isotropic hardening and softening has been proposed by Mühlhaus. It differs from the conventional elasto-plastic law of Drucker-Prager in the presence of Cosserat rotations

and couple stresses using the mean grain diameter as a characteristic length. It can be summarised as follows:

$$\dot{\varepsilon}_{ij} = \dot{\varepsilon}^e_{ij} + \dot{\varepsilon}^p_{ij}, \qquad \dot{\kappa}_i = \dot{\kappa}^e_i + \dot{\kappa}^p_i, \tag{13}$$

$$\dot{\varepsilon}^e_{ij} = \frac{1}{E}[(1+v)\dot{\sigma}_{ij} - v\dot{\sigma}_{kk}], \qquad i = k, \tag{14}$$

$$\dot{\varepsilon}^e_{ij} = \frac{1}{2G}\frac{\partial \dot{\tau}^2}{\partial \sigma_{ij}}, \qquad \dot{\kappa}^e_i = \frac{1}{2G}\frac{\partial \dot{\tau}^2}{\partial m_i}, \qquad i \neq j, \tag{15}$$

$$\dot{\varepsilon}^p_{ij} = \lambda\frac{\partial g}{\partial \sigma_{ij}}, \qquad \dot{\kappa}^p_i = \lambda\frac{\partial g}{\partial m_i}, \tag{16}$$

$$\tau = (a_1 s_{ij}s_{ij} + a_2 s_{ij}s_{ji} + \frac{a_3}{d_{50}^2} m_i m_i)^{0.5}, \tag{17}$$

$$f = \tau + \mu(e_0, \gamma^p)p - c, \tag{18}$$

$$g = \tau + \alpha(e_0, \gamma^p)p, \tag{19}$$

wherein τ is the second invariant of the deviatoric stress tensor, s_{ij} – the non-symmetric deviatoric stress tensor ($s_{ij} = \sigma_{ij} - p\delta_{ij}$), p – mean stress, σ_{ij} – the stress tensor, m_i – the couple stress vector, a_1, a_2, a_3 – coefficients, d_{50} – mean grain diameter, f – the yield function, g – the potential function, μ – the mobilised friction factor, α – the mobilised dilatancy factor, c – cohesion, e_0 – the initial void ratio, γ^p – plastic shear deformation, ε_{ij} – the deformation tensor, $\dot{\varepsilon}_{ij}$ – the rate of deformation tensor, κ_i – the curvature vector, $\dot{\kappa}_i$ – the rate of curvature vector, λ – the proportionality factor, E – the elastic modulus, G – the shear modulus, v – the Poisson ratio, δ_{ij} – the Kronecker delta. The superimposed indexes e and p designate the elastic and the plastic strain or curvature, respectively. The factors μ in Equation (18) and α in Equation (19), which are related to the angle of internal friction, ϕ, and the angle of dilatancy, β, of granular materials, can be identified with the help of tests in a plane strain or in a triaxial apparatus.

Figure 11 shows the evolution of the mobilised friction factor, μ, and the mobilised dilatancy factor, α, for granular materials. The functions describing the mobilised friction factor, μ, and mobilised dilatancy factor, α, versus plastic shear deformation, γ^p, were proposed on the basis of biaxial tests.

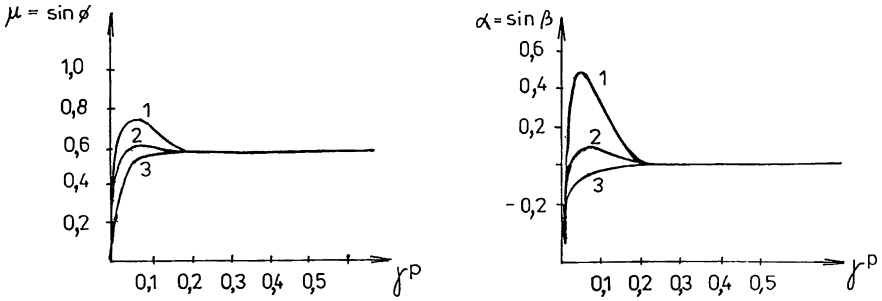

Figure 11. Mobilised friction factor, μ, and mobilised dilatancy factor, α, for dense granular materials (ϕ – angle of internal friction, β – dilatancy angle, γ^p – plastic shear deformation); 1 – dense, 2 – medium dense, 3 – loose material

5. FE input data

To simulate resonance effects during silo flow in a silo with parallel walls, a system containing bulk solid (sand) and two walls was assumed. A total of 960 triangular finite elements were applied (800 for the solid and 80 for each wall). The silo walls of perspex (with a thickness of $t_w = 5\,\mathrm{mm}$) were assumed to behave purely elastically (elastic modulus of walls $E_w = 3\,300\,000\,\mathrm{kPa}$, Poisson's ratio for walls ($v = 0.3$). For the sake of simplicity, plane strain mass flow in a model silo was taken into account with a controlled outlet velocity ($v_f = 5\,\mathrm{mm/s}$) along the bottom between two parallel smooth walls (silo height $h = 2.0\,\mathrm{m}$, silo width $b = 0.2\,\mathrm{m}$, see [6, 7]). This type of flow has been observed in experiments in a cylindrical model in the upper part of the silo.

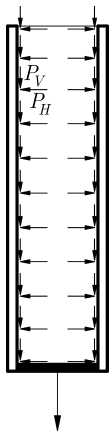

Figure 12. System assumed for numerical simulations of resonance effects ($P_{H,V}$ – horizontal and vertical nodal forces along walls)

Horizontal wall displacements and horizontal displacements in the bulk solid along the contact surface were assumed to be equal ($u_1^w = u_1^m$, see Figure 12). At the interface, a polar wall boundary condition was introduced to describe wall roughness of smooth walls ($r_w \ll d_{50}$): $\omega^c / u_2 = r_w / d_{50}^2$ with $r_w / d_{50} = 0.05$, wherein ω^c is Cosserat rotation, u_2 – vertical displacement, d_{50} – mean grain diameter, and r_w – wall roughness. As an initial stress state, stresses after filling were assumed according to the slice method proposed by Janssen. Along the entire bottom, constant vertical displacements were prescribed ($u_1 = 0$, $\omega^c = 0$, $u_2 = n\Delta u$), wherein u_1 was horizontal displacement, n – step number, Δu – an increment of bottom displacement.

An updated Lagrangian approach was adopted in the formulation of the incremental form of the governing equations. To solve the non-linear equation of motion governing the response of a system of finite elements, an implicit integration method proposed by Newmark was used with a modified Newton-Raphson scheme. The calculations were performed using a symmetric, elastic global stiffness matrix. The time increment dt was chosen as 0.0005s. In this range, the effect of dt was found to be insignificant.

6. Numerical results

First, FE calculations of solid flow without walls were performed (model silo: $h = 2.0\,\mathrm{m}$, $d = 0.2\,\mathrm{m}$, and large silo: $h = 20.0\,\mathrm{m}$, $d = 2.0\,\mathrm{m}$), assuming that horizontal displacements along the vertical boundaries of the material were equal to zero. For the sand in silo model, the following material parameters were assumed: $\gamma_d = 17.0\,\mathrm{kN/m^3}$ (initial density), $E_m = 50\,000\,\mathrm{kPa}$ (elastic modulus), $\overline{K} = 0.22$ (pressure coefficient at filling), $\varphi_w = 15^\circ$ (wall friction angle at filling), $v = 0.3$ (Poisson's ratio), $\phi_{\max} = 40^\circ$ (maximum internal friction angle), $\phi_{\mathrm{cr}} = 35^\circ$ (residual internal friction angle), $\beta_{\max} = 28.3^\circ$ (maximum dilatancy angle), $\beta_{\mathrm{cr}} = 0^\circ$ (residual dilatancy angle), $\gamma_p^p = 0.05$ (maximum plastic shear deformation), $\gamma_{\mathrm{cr}}^p = 0.20$ (residual plastic shear deformation), $a_1 = 0.375$, $a_2 = 0.125$ and $a_3 = 0.25$ (micro-polar coefficients). For sand in a large silo, the parameters were: $\gamma_d = 17.00\,\mathrm{kN/m^3}$, $E_m = 100\,000\,\mathrm{kPa}$, $\overline{K} = 0.22$, $\varphi_w = 15^\circ$, $v = 0.3$, $\phi_{\max} = 37^\circ$, $\phi_{\mathrm{cr}} = 35^\circ$, $\beta_{\max} = 19^\circ$, $\beta_{\mathrm{cr}} = 0^\circ$, $\gamma_p^p = 0.10$, $\gamma_{\mathrm{cr}}^p = 0.20$, $a_1 = 0.375$, $a_2 = 0.125$, $a_3 = 0.25$.

The results of numerical simulations indicate that the amplitudes of the normalised horizontal wall stress are similar in large and small silos (Figure 13). The calculated basic frequency of pulsations was 25 Hz (model silo) and 3.75 Hz (large silo). The same frequencies can also be obtained with Equation (2).

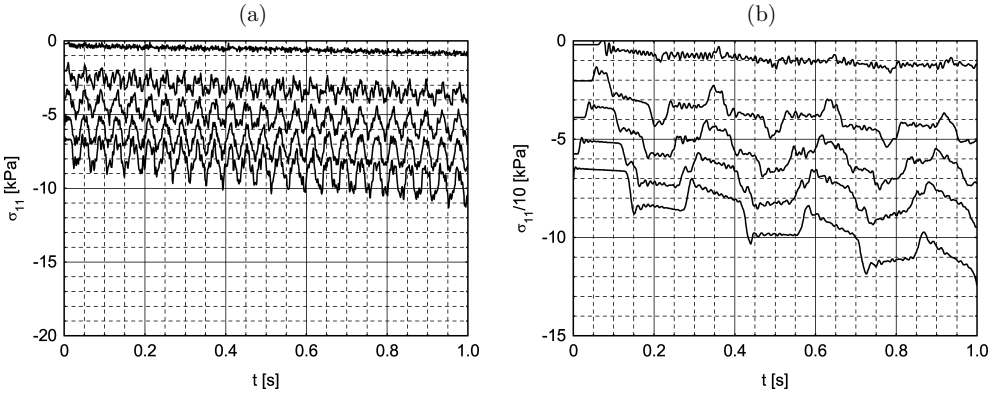

Figure 13. Calculated horizontal normal stresses along the wall, σ_{11}, during flow in a model silo with controlled outlet velocity: (a) model silo $v = 5\,\mathrm{mm/s}$, $h = 2.0\,\mathrm{m}$, $b = 0.2\,\mathrm{m}$, $d_{50} = 0.5\,\mathrm{mm}$; (b) large silo $v = 50\,\mathrm{mm/s}$, $h = 20.0\,\mathrm{m}$, $b = 2.0\,\mathrm{m}$, $d_{50} = 0.5\,\mathrm{mm}$

Since it is difficult to adjust the natural frequencies of bulk solid to the natural frequencies of the entire system (bulk solid and walls), the bulk solid along the wall contact line was additionally excited with small harmonic vertical and horizontal dynamic forces to investigate the effect of resonance on wall stresses (Figure 12). The harmonic forces were equal to:

$$P_{H,V} = P_0^{H,V}(\sin 2\pi f_{\mathrm{ext}} t), \tag{20}$$

where $P_0^{H,V}$ was amplitude of vibrations, f_{ext} – frequency of excitation, and t – time. The vibration amplitude of the forces was assumed to be one-tenth of forces calculated for the filling state according to Janssen. Thus, these forces were small enough not to influence the wall stresses beyond the resonance region. The excitation frequencies

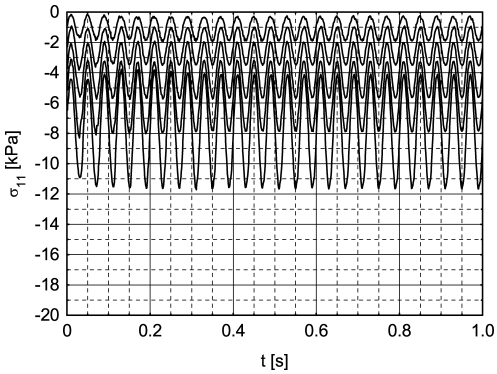

Figure 14. Calculated horizontal normal stresses along the wall, σ_{11}, during flow in a model silo with controlled outlet velocity ($v = 5$mm/s, $E_w = 3\,300\,000$kPa, $h = 2.0$m, $b = 0.2$m, $t_w = 5$mm, $f_{\text{ext}} = 25$Hz)

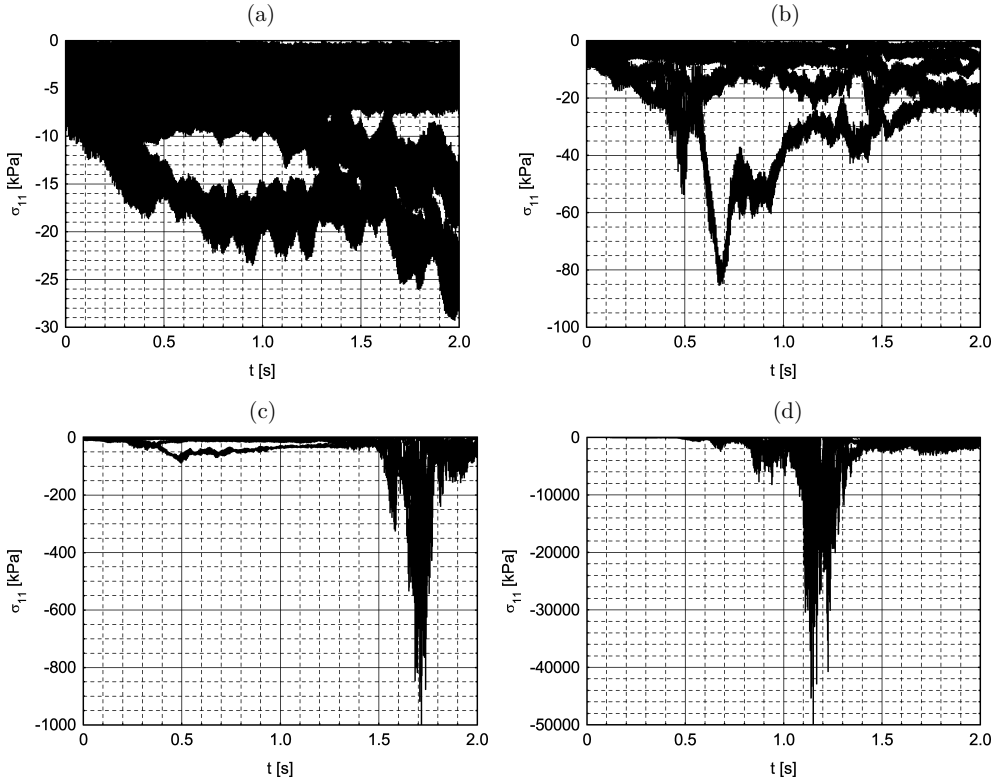

Figure 15. Calculated horizontal normal stresses along the wall, σ_{11}, during flow in a model silo with controlled outlet velocity for various excitation frequencies: (a) $f_{\text{ext}} = 180$Hz; (b) $f_{\text{ext}} = 200$Hz; (c) $f_{\text{ext}} = 206$Hz; (d) $f_{\text{ext}} = 222$Hz ($v = 5$mm/s, $E_w = 3\,300\,000$kPa, $h = 2.0$m, $b = 0.2$m, $t_w = 5$mm)

of the forces, f_{ext}, were assumed to be equal to frequencies of natural vibrations of a single silo wall (case 1), of the bulk solid (case 2) and of the whole system consisting of a bulk solid between two silo walls (case 3), Table 1. The natural frequencies were determined twofold: by eigen-value analysis of the matrix $[A] = [K]^{-1}[M]$ ($[K]$ – global

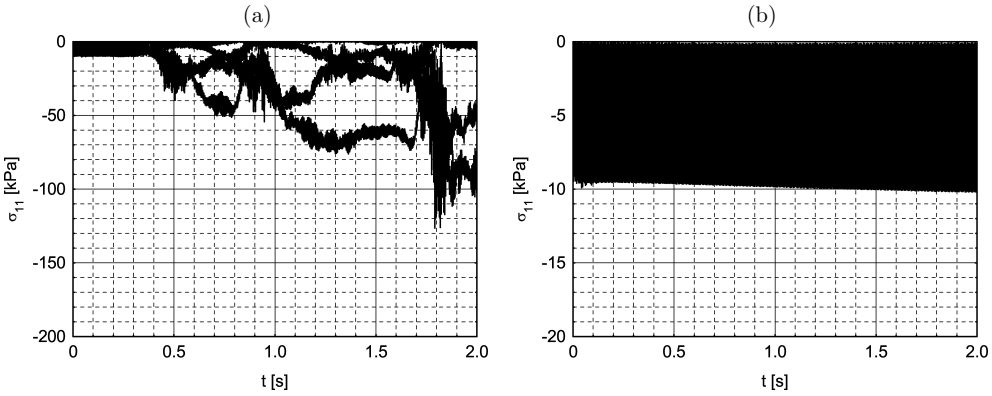

Figure 16. Calculated horizontal normal stresses along the wall, σ_{11}, during flow in a model silo with controlled outlet velocity: (a) wall damping coefficient $\alpha = 200\text{s}^{-1}$; (b) wall damping coefficient $\alpha = 300\text{s}^{-1}$ ($v = 5\text{mm/s}$, $E_w = 3\,300\,000\text{kPa}$, $h = 2.0\text{m}$, $b = 0.2\text{m}$, $t_w = 5\text{mm}$, $f_{\text{ext}} = 206\text{Hz}$)

stiffness matrix, $[M]$ – global mass matrix) and by spectral analysis of displacements, velocities, accelerations and stresses obtained by the excitation of the wall, the bulk solid and the entire system with a single vertical and horizontal force. For the first two cases, no increase of horizontal normal wall stresses took place.

Table 1. Calculated natural frequencies in a model silo

Component	Natural frequencies [Hz]
single wall	11, 67, 184,… (horizontal excitation) 200, 367,… (vertical excitation)
bulk solid	25, 75, 125, 175, 225,… (vertical excitation)
system: bulk solid + walls	1.32, 6.33, 22.00, 44.93, 45.63, 77.68, 89.80, 116.60, 134.70, 160.40, 179.80, 206.20, 222.00, 225.60, 250.00, 289.90, 410.10, 486.60,…

Figure 14 presents the evolution of horizontal normal stresses at various points along the wall during flow with a frequency of excitation equal to 25Hz (the basic natural frequency of the bulk solid in the vertical direction, Equation (2)). In the case of excitation with frequencies corresponding to the frequencies of natural vertical vibrations under vertical excitation of the whole system (case 3), an infinitely large increase of wall stresses was obtained due to resonance. The increase of wall stresses occurred at frequencies of excitation $f_{\text{ext}} \geq 180\text{Hz}$ (Figure 15).

The rate of increase of the wall stresses diminished with an increase of the damping coefficient of the silo walls, α. The α coefficient was calculated according to the following formula:

$$\alpha = 2\omega D = 4\pi f D, \tag{21}$$

where f is the frequency of vibrations and D denotes the damping ratio. Assuming that $f = 206\text{Hz}$ and $D = 0.08$ (perspex), the damping coefficient is equal to $\alpha \cong 200\text{s}^{-1}$. In this case, an increase in wall stresses due to resonance was significantly limited (Figure 16a). When the damping coefficient was larger, $\alpha = 300\text{s}^{-1}$, the resonance effect was completely suppressed (Figure 16b).

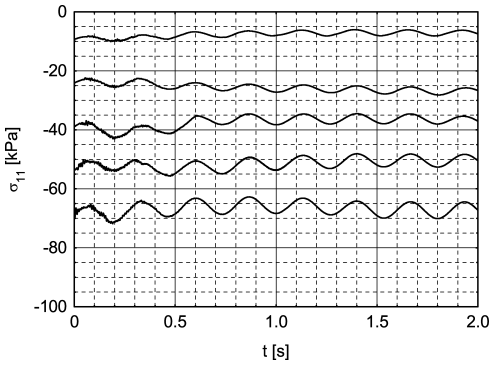

Figure 17. Calculated horizontal normal stresses along the wall, σ_{11}, during flow in a large silo with controlled outlet velocity ($v = 50\,\text{mm/s}$, $E_w = 3\,300\,000\,\text{kPa}$, $h = 20.0\,\text{m}$, $b = 2.0\,\text{m}$, $t_w = 5\,\text{mm}$, $f_{\text{ext}} = 3.75\,\text{Hz}$)

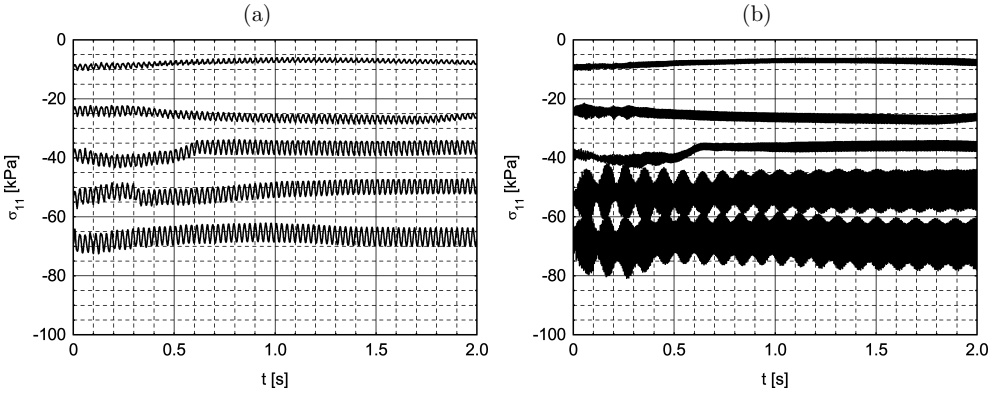

Figure 18. Calculated horizontal normal stresses along the wall, σ_{11}, during flow in a large silo with controlled outlet velocity for various excitation frequencies: (a) $f_{\text{ext}} = 35\,\text{Hz}$; (b) $f_{\text{ext}} = 186\,\text{Hz}$ ($v = 50\,\text{mm/s}$, $E_w = 3\,300\,000\,\text{kPa}$, $h = 20.0\,\text{m}$, $b = 2.0\,\text{m}$, $t_w = 5\,\text{mm}$)

FE calculations were also carried out for a large plane strain silo ($h = 20.0\,\text{m}$, $b = 2.0\,\text{m}$, $t_w = 5\,\text{mm}$, $v = 50\,\text{mm/s}$, medium dense sand). The effect of higher pressure on the internal friction angle, the dilatancy angle and the elastic modulus of the bulk solid was taken into account ($E_m = 100\,000\,\text{kPa}$, $\phi_{\max} = 37^\circ$, $\phi_{\text{cr}} = 35^\circ$, $\beta_{\max} = 4^\circ$). As in the case of the model silo, the amplitude of forces $P_{H,V}$ (Equation (20)) was one-tenth of the forces calculated for the filling state. The excitation frequencies were assumed again to be equal to the natural frequencies of a single wall, the bulk solid and the entire system of the bulk solid and the silo walls. Figure 17 presents the evolution of horizontal normal stresses at various points along the wall during flow with the frequency of excitation equal to 3.75 Hz (the basic natural frequency of the bulk solid in the vertical direction according to Equation (2)). Figure 18a presents the results obtained for the frequency of excitation equal to 35 Hz (the natural frequency of the whole system in the horizontal direction), and Figure 18b – for the frequency of excitation of 186 Hz (the natural frequency of the entire system in the vertical excitation direction). The increase of wall stresses in the large silo due to resonance was significantly smaller than in the model silo (only by about 10%).

7. Conclusions

During the process of silo emptying, strong dynamic effects can be created due to resonance between the bulk solid and the silo structure. The resonance effects occur in silos with thin, smooth walls containing both cohesive and non-cohesive bulk solids during mass flow and channel flow at the wall.

The resonance effects can considerably increase wall pressures in small silos. Their increase is influenced by the type and velocity of flow, material cohesion, grain stiffness and wall roughness.

The most reliable and practical method of reducing the dynamic phenomena in cohesive and non-cohesive bulk solids during silo flow and to suppress the resonance effects is to increase wall roughness above the transition between mass and channel flow.

The frequency of resonance effects is related to the frequency of natural vertical vibrations of the entire silo structure containing the silo fill.

The effect of resonance on wall pressures diminishes with increasing size of silos and damping properties of silo walls.

References

[1] Tejchman J and Gudehus G 1993 *Powder Technology* **76** (2) 201
[2] Roberts A W 1995 *Proc. 3rd Europ. Symp. Storage and Flow of Particulate Solids*, Nürnberg, pp. 131–141
[3] Hardow B, Schulze D and Schwedes J 1998 *Proc. World Congress for Particle Technology*, Nürnberg, Germany, pp. 11–19
[4] Tejchman J 1997 *Publication Series of the Institute of Soil Mechanics and Rock Mechanics*, Karlsruhe University, pp. 1–283
[5] Tejchman J 1999 *Powder Technology* **106** 7
[6] Niedostatkiewicz M 2003 *Dynamic Effects in Silos*, PhD Thesis, Gdansk University of Technology, Gdansk, pp. 1–258 (in Polish)
[7] Niedostatkiewicz M and Tejchman J 2003 *Powder Handling and Processing* **15** (1) 36
[8] Tejchman J 2001 *Int. J. Storing, Handling and Processing Powder* **13** (2) 165
[9] Mühlhaus H B 1989 *Ing. Arch.* **59** 124
[10] Tejchman J 1998 *Thin-Walled Structures* **31/1-3** 137